FULL PAPER

High-Efficiency Organic Solar Cells Based on Preformed Poly(3-hexylthiophene) Nanowires

*Jong Soo Kim, Ji Hwang Lee, Jong Hwan Park, Chiyeoung Shim, Myungsun Sim, and Kilwon Cho**

Bulk heterojunction solar cells based on blends of poly(3-hexylthiophene) (P3HT) and phenyl-C61-butyric acid methyl ester ($PC_{61}BM$) are fabricated using self-assembled P3HT nanowires in a marginal solvent without post-treatments. The interconnected network structures of self-organized P3HT nanowires create continuous percolation pathways through the active layer and contribute to enhanced carrier mobility. The morphology and photovoltaic properties are studied as a function of ageing time of the P3HT precursor solution. Optimal photovoltaic properties are found at 60 h ageing time, which increases both light absorption and charge balance. Multilayered solar cells with a compositionally graded structure are fabriacted using preformed P3HT nanowires by inserting a pure P3HT donor phase onto the hole-collecting electrode. Applying optimized annealing conditions to the P3HT buffer layer achieves an enhanced hole mobility and a power conversion efficiency of 3.94%. The introduction of a compositionally graded device structure, which contains a P3HT-only region, reduces charge recombination and electron injection to the indium tin oxide (ITO) electrode and enhances the device properties. These results demonstrate that preformed semiconductor nanowires and compositionally graded structures constitute a promising approach to the control of bulk heterojunction morphology and charge-carrier mobility.

1. Introduction

Recently, much effort has been devoted toward obtaining high-efficiency, bulk heterojunction (BHJ), organic photovoltaic (OPV) devices that are easily processed, mechanically flexible, and have low fabrication costs for large area devices.[1–4] With the demands for new materials that have enhanced properties, such as a narrow band gap and high carrier mobility, control over the interface and morphology of the active layer are key issues for achieving high efficiency OPVs. In particular, control over the nanoscale phase separation between the donor and acceptor, molecular ordering enhancement of the donor polymers, and an increase in the percolation of acceptor molecules are critical factors that determine BHJ device properties. Device efficiency is mainly determined by control over the nanostructure of the donor–acceptor blended active layer. A large interface[5] between the donor and acceptor layers is needed for the dissociation of excitons, and efficient charge extraction requires a nanostructure that allows efficient charge transport to the electrodes.

Many studies have investigated the optimization of nanostructures for BHJs by controlling the preparation process of the active layer,[6–8] introducing post-treatments via thermal kinetics or solvent reorganization,[9–13] or controlling the interface by changing the surface energy or the work function.[14,15] In particular, BHJ solar cells composed of P3HT and PCBM are being intensively investigated.[16,17] However, P3HT/PCBM BHJ solar cells have several disadvantages for organic solar cell applications, for example, morphology optimization, low hole mobility, and the absence of a pure donor phase at the hole-collecting electrode where recombination and incorrect charge injection may occur.

Several approaches to controlling the nanoscale morphology and enhancing the carrier mobility of P3HT/PCBM blend solar cells (the carrier mobility mainly affects exciton diffusion and charge transfer) have been reported.[18,19] Recently, the Jenekhe group reported a preparation of a poly(3-butylthiophene) (P3BT) nanowire/PCBM blend solar cell that showed enhanced hole mobility via the formation of nanowires.[20,21] They obtained an efficiency of 3% without the application of post-treatments. However, despite efforts to control the carrier mobility and morphology, optimization of BHJ device structures remains a challenge. Moreover, multilayered photovoltaic devices with a pure donor component layer at the anode and a composition gradient throughout the blend film have received only limited attention to date. With the exception of the tandem cell, it is not easy to control layer thickness on the scale of nanometers or to identify selective solvents for multilayer deposition, mainly because the undercoated layer is damaged during subsequent overcoating steps.

Here, we demonstrate the use of self-assembled P3HT nanofiber/PCBM network structures (**Figure 1**b), prepared after

Dr. J. S. Kim, Dr. J. H. Lee, J. H. Park, C. Shim, M. Sim, Prof. K. Cho
School of Environmental Science and Engineering
Department of Chemical Engineering
Polymer Research Institute
Pohang University of Science and Technology
Pohang, 790–784, Korea
E-mail: kwcho@postech.ac.kr

DOI: 10.1002/adfm.201000971

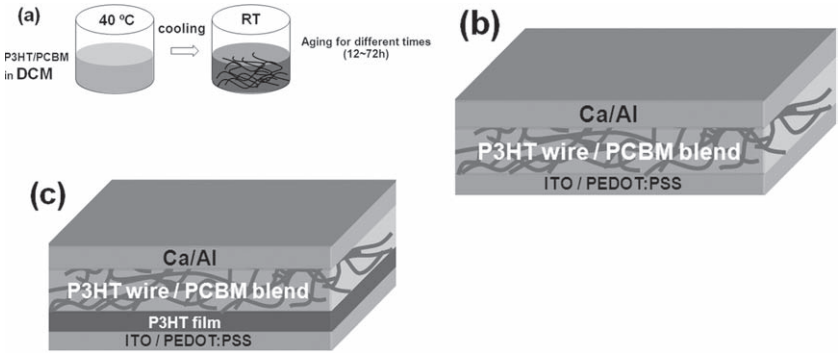

Figure 1. a) Scheme illustrating the preparation of blend solutions of P3HT nanowires and PCBM via thermal treatment. Device structures used in this study: b) Active layer fabricated from solutions with different ageing times (12h, 24h, 36h, 48h, 60h, 72h); c) P3HT layer insertion with annealing process (untreated, 100 °C, 150 °C, 200 °C, 250 °C).

ageing the nanofiber precursor solution for different times. For solution recrystallization, ageing was shown to enhance charge transport and network connectivity, and to optimize the efficiency of bulk heterojunction solar cell devices. The crystallinity and optical properties of the nanofibers were measured after different ageing times and the ageing time was correlated with the photovoltaic properties. Application of the optimized ageing time and device structures yielded enhanced device performances without the use of post-treatments. Using the optimally-aged preformed P3HT nanowires, a compositionally graded OPV cell that contained a thermally annealed pure P3HT layer as the buffer layer at the indium tin oxide (ITO) electrode was fabricated (Figure 1c). By using P3HT nanowires and an inserted-P3HT-layer device structure, enhanced carrier mobility and a balance between the charge mobilities of the electron and hole were achieved, contributing to more efficient charge transport, which reduces series resistance and induces a higher fill factor for higher solar cell efficiency.

2. Results and Discussion

Figure 2a shows the temperature-dependent UV-vis absorption spectra of homo-P3HT in dichloromethane (DCM). As the temperature decreases to room temperature, the absorption peaks at λ = 518, 552 and 605 nm appear. These wavelength regions correspond to absorption by the highly-conjugated π–π interaction. Simultaneously, the absorption at λ = 450 nm, the representative region for the freely-dissolved P3HT chains, decreases and disappears, and the absorption peak maximum red-shifts, indicating that the P3HT chains have gradually solidified. These effects are mainly caused by the temperature-dependent solubility of P3HT in DCM, which is a marginal solvent for P3HT.[22,23] The majority of P3HT chains were assembled in the DCM solution at room temperature and formed nanowires as the solubility of P3HT decreased. For blends containing this solution and PCBM, the absorption spectra show two clear peaks: one at 335 nm corresponding to PCBM, and another at 500 nm-550 nm representing the contributions of P3HT in Figure 2b. The spectra show pronounced red-shifts and growth of new absorption bands as the temperature was decreased, whereas the PCBM peak remains unchanged. The P3HT nanowire/PCBM blend solution was used to fabricate the OPV active layer.

The morphology of P3HT nanowire/PCBM blend films was investigated using TEM and AFM. P3HT nanowires 10 nm in width and 5–10 μm in length were observed in both the TEM and AFM images (**Figure 3**). These nanowires form an interconnected network surrounded by a continuous PCBM phase, together constituting a bicontinuous nanoscale morphology that enlarges the contact area between the P3HT nanowires and the PCBM for enhanced charge separation.

The light absorption properties and crystal structure of the active layer were measured using solid UV–vis spectroscopy and grazing incidence X-ray diffraction (GI-XRD) (**Figure 4**). The absorption spectra of the P3HT nanowire/PCBM spin-coated film are shown in Figure 4a as a function of the solution ageing time. Similar to the results from the solution UV measurement, three absorption peaks at 520, 552, and 605 nm were observed. The latter vibronic peaks are due to strong π–π stacking within the assembled P3HT nanowires. As expected, the two vibronic features at 552 and 605 nm in the film appear at the same wavelengths as those in the solution UV absorption spectrum of P3HT. The nanowire is the fully developed structure; therefore the red-shift based on the increase of the polymer-chain stacking looks quite weak. An increase in the peak intensities corresponding to the π–π stacking regions near 552 and 605 nm show increased P3HT assembly with an increase of the ageing time. Figure 4b shows the XRD data, which agrees with the UV absorption results. The observed P3HT (100) peaks, with higher order peaks along the q_z axis, suggested that P3HT molecules adopt edge-on structures in which the (100) axis is normal to the substrate. This conclusion is supported by the near-edge X-ray adsorption fine structure spectroscopy (NEXAFS) spectra shown in Figure S1. The intensity of the P3HT (100) peak increased gradually as the ageing time increased, however, at an

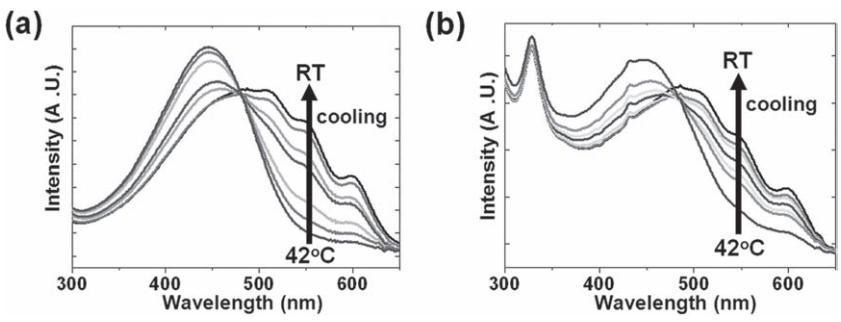

Figure 2. UV–vis absorption spectra of (a) homo-P3HT and (b) P3HT/PCBM (1:1) solution in DCM as a function of the temperature, from 42 °C to room temperature.

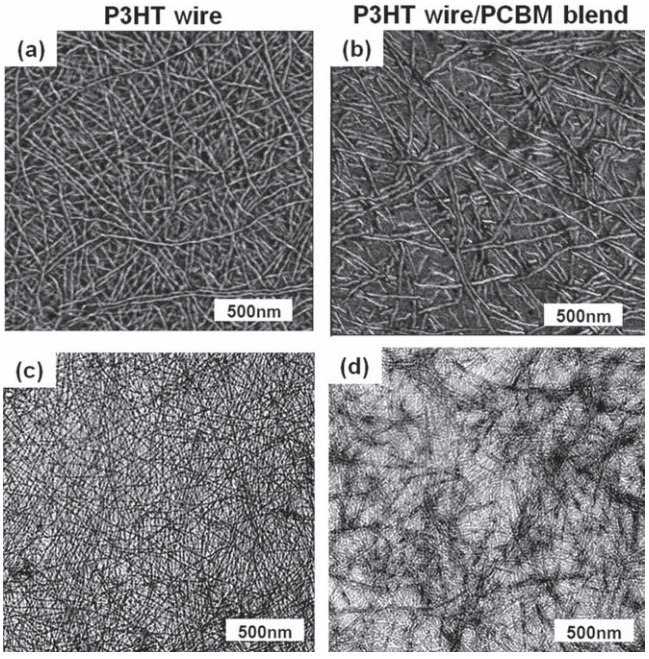

Figure 3. AFM and TEM images, respectively, of (a,c) homo-P3HT nanowires and (b,d) P3HT nanowires/PCBM blend film.

ageing time of 60 h, the intensity was saturated. This may have been caused by the saturation of P3HT nanowires formation above 60 h.

Photovoltaic cells incorporating P3HT nanowires/PCBM as the active layer were fabricated over an area of 5.15 mm^2, and device properties were measured at 100 $mW \cdot cm^{-2}$, AM 1.5 conditions in an inert N_2 environment. The device structure consisted of a multilayered structure, ITO/PEDOT:PSS/P3HT nanowires:PCBM/Ca/Al. **Figure 5**a compares the current-density–voltage (J–V) curves of P3HT nanowires/PCBM solar cell devices as a function of the ageing time of the nanowire solution. The photovoltaic parameters, such as the short circuit current density (J_{sc}), open circuit voltage (V_{oc}), fill factor (FF), power conversion efficiency (PCE), and carrier mobilities are summarized in **Table 1**. The performance of the photovoltaic cells was found to depend greatly on the ageing time of the nanowire solution. At an ageing time of 12 h, a power conversion efficiency of 1.78% was obtained. When the ageing time was increased to 72 h, the efficiency increased to 3.03%. The best performance was achieved from the 60 h aged solution, in which V_{oc} = 0.59, J_{sc} = 9.51, FF = 0.58, and the power conversion efficiency was 3.23%. For the measurements of power conversion efficiency, the incident photon-to-current efficiency (IPCE) was investigated in relation to the ageing time. IPCE data in Figure 5b reflects a similar efficiency dependence on ageing time. IPCE increased from 43% to a maximum of 62% as the ageing time was increased, and the value of IPCE was similar to that observed in the (J–V) curves. The relationship between ageing time and photovoltaic properties was examined by plotting J_{sc}, V_{oc}, FF, and PCE as a function of ageing time (**Figure 6**). As shown in Figure 6a, enhanced power conversion efficiencies reflect the dependence of the short circuit current density on ageing time, indicating that the PCE of the P3HT nanowires/PCBM blend solar cell was dominated by J_{sc}. This dependence can be understood in terms of the relatively similar V_{oc} and FF (Figure 6b) in the P3HT nanowires/PCBM blend solar cells. Because J_{sc} is the result of the light absorption, exciton dissociation and charge transport are also critical to the overall PCE.

An increase in J_{sc} mainly affected the PCE; therefore, the charge transport properties of the device were studied. The hole and electron mobilities of the P3HT nanowires/PCBM blend film were investigated as a function of ageing time using space charge limit current (SCLC) measurements with electron-only/hole-only devices. **Figure 7**a shows the dark currents of ITO/PEDOT:PSS/P3HT nanowires:PCBM/Pd devices[24–25] with the corrected bias, which was determined as the difference between the work function of Pd and the HOMO level of P3HT. Electron-only devices (Al/P3HT nanowires:PCBM/Al) were fabricated, and the dark J–V characteristics were investigated, as shown in Figure 7b. In the trap-free region over the trap-filled limit, which is the limit of the presence of carrier traps, SCLC behavior can be characterized by the Mott–Gurney square law (Equation (1)),

$$J = (9/8)\varepsilon\mu(V^2/L^3) \quad (1)$$

where ε is the static dielectric constant of the medium, i.e., the organic layer, and μ is the charge carrier mobility.[26] The hole mobility calculated from the currents in the square law region gradually increases from 10^{-6} to 10^{-5} as the ageing time is increased. In the P3HT nanowires/PCBM device, the hole carrier separated from the exciton and moved into the ITO through the P3HT nanowires and the electron passed through the PCBM domains. Therefore, the hole-mobility enhancement at longer solution ageing times is caused by enhanced π–π stacking and chain ordering, as supported by the UV and XRD data. However, whereas the hole mobility increases by one order of magnitude, the electron mobility does not increase significantly (it remains on the order of 10^{-4}, Table 1). This observation shows that the PCBM domain and cluster regions remain as prepared, regardless of the solution ageing time, to produce similar electron mobilities.

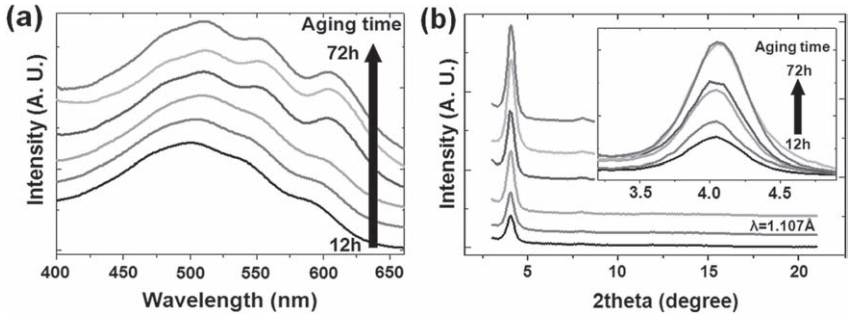

Figure 4. a) UV–vis absorption spectra and (b) GI- XRD patterns of P3HT nanowires/PCBM blend (0.4 wt%, 1/1) films at a grazing angle of 0.18° on an ITO/PEDOT:PSS substrate with various ageing times, from 12 h to 72 h.

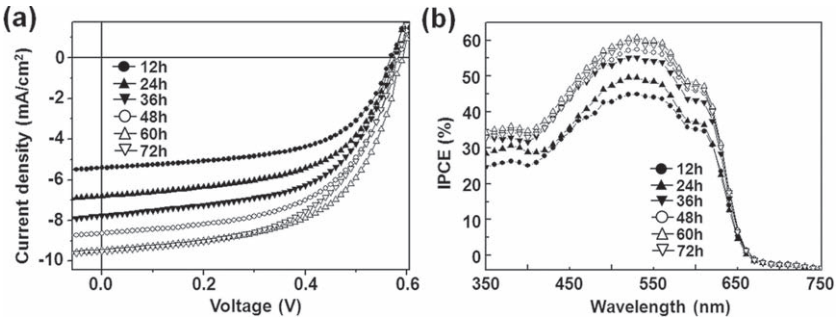

Figure 5. a) The current-voltage characteristics and b) IPCE data for solar cells composed of P3HT nanowires/PCBM blend films with various ageing times, from 12 h to 72 h.

With the hole mobility enhancement and a similar electron mobility, a carrier mobility balance between holes and electrons could be achieved (Table 1), which reduced the space charges resulting in the improvement of the photovoltaic properties. The best ageing time of the precursor solution for the devices was 60 h allowing the resulting ratio between the electron and hole mobilities to approach unity (μ_e/μ_h = 1.4), yielding balanced carrier transport in the active layer. When the charge transport in the device is unbalanced (for example, in the pristine P3HT/PCBM blend system where μ_h is significantly lower than μ_e), hole accumulation occurred in the device and the photocurrent was space-charge limited.[9]

The exciton dissociation efficiency of these devices was also studied. The generation rate of free carriers (G) is described by Equation (2),

$$G(T, E) = G\max \mathrm{P}(T, E) \quad (2)$$

where G_{max} is the maximum generation rate of bound electron–hole pairs, P(T, E) is the probability for charge separation at the donor–acceptor interface,[27,28] limited by temperature (T) and the electrical field (E). Because the photocurrent can be determined by the rate of generation of free carriers, which is governed by the probability of charge separation,[26–29] the exciton dissociation efficiency, similar to the probability of charge separation, is an important process for enhancing device performance. Therefore, the P(T, E) of each aged P3HT nanowire/PCBM blend device was compared to derive the J_{sc} increase. Figure 7c shows a log–log plot of the photocurrent ($J_{ph} = J_L - J_D$) arising from the devices' J–V curves of the P3HT nanowires:PCBM as a function of the effective applied voltage (V_0–V) with different ageing times. The photocurrent could be estimated by $J_{ph} = eG(T, E)L$ in the saturation regime for (V_0–V) > 0.3–0.4 V, where e is the electrical charge, L is film thickness. Most bound electron–hole pairs were separated into free carriers and the photocurrent was saturated at $J_{sat} = eG_{max}L$ in the region of high voltages (> 1 V).[28] Under short circuit conditions, the value of J_{sc}/J_{sat}[27] exceeded 0.9 and was not significantly different for different ageing times (Table 1). Recombination is also an important process to charge separation efficiency and has a strong influence on charge extraction. However, in cases where J_{sc}/J_{sat} > 0.9, charge extraction is much more efficient than charge recombination. Particularly in our devices, the charge extraction process is more efficient than recombination because the values of J_{sc}/J_{sat} are in the range of 0.93–0.98, which is close to unity.

However, the saturation current, J_{sat}, of the 12 h-aged device was only 60% of that of the 60 h aged devices (Figure 7c, Table 1). As mentioned, because most of the bound electron–hole pairs are separated into free carriers in the saturated regime, G_{max} is mainly governed by the quantity of absorbed photons. Similar to the results described by Blom,[27] the gradual increase in G_{max} of the device from the aged solution results entirely from the enhanced absorption, implying that almost all of the excitons generated in the P3HT nanowire phase of the blend dissociated at the D-A interface and formed electron–hole pairs. This conclusion is supported by the UV absorption data (Figure 4a), which demonstrates that increased light absorption intensity enhances the photocurrent. Although a slight red-shift is observed in the light absorption upon ageing the P3HT nanowire solution, the net effect of the red-shift and increase in intensity is an improvement of the spectral overlap with solar emission, which contributes to the increase in the light absorption.[24]

Longer ageing times of the P3HT precursor solution increase the conjugation length and crystallinity of self-assembled P3HT. The crystallinity of P3HT is a critical factor for enhancing the hole mobility of P3HT. π-orbital overlapping, induced by π–π stacking, amplifies electron delocalization so that the carriers move more easily through the overlapping orbital pathways. As a consequence, the enhanced hole mobility balances with the electron mobility and reduces charge accumulation in the

Table 1. Photovoltaic properties, charge carrier mobility of P3HT nanowires/PCBM blend films as a function of the solution ageing time. (t: thickness, V_{oc}: open circuit voltage, J_{sc}: short circuit current density, FF: fill factor, η: efficiency, J_{sat}: saturated photocurrent, η_{CT}: charge transfer efficiency, G_{max}: maximum photogenerated rate of bound electron-hole pairs, μ_h: hole mobility, μ_e: electron mobility)

Ageing time [h]	t [nm]	V_{oc} [V]	J_{sc} [mA·cm^{-2}]	FF	η [%]	J_{sat}	η_{CT}	G_{max}	μ_h [cm^{2}V^{-1}s^{-1}]	μ_e [cm^{2}V^{-1}s^{-1}]	μ_e/μ_h
12	74	0.57	5.42	0.58	1.78	5.77	0.94	1	3.37×10^{-6}	2.23×10^{-4}	66.2
24	78	0.57	6.79	0.57	2.21	7.30	0.93	1.27	8.12×10^{-6}	1.28×10^{-4}	15.7
36	75	0.58	7.76	0.56	2.53	8.26	0.94	1.43	1.27×10^{-5}	2.25×10^{-4}	17.7
48	78	0.58	8.63	0.57	2.83	9.18	0.94	1.59	2.91×10^{-5}	2.00×10^{-4}	6.8
60	81	0.59	9.51	0.58	3.23	9.71	0.98	1.68	8.50×10^{-5}	1.18×10^{-4}	1.4
72	85	0.58	9.54	0.55	3.03	9.84	0.97	1.71	8.80×10^{-5}	2.88×10^{-4}	3.3

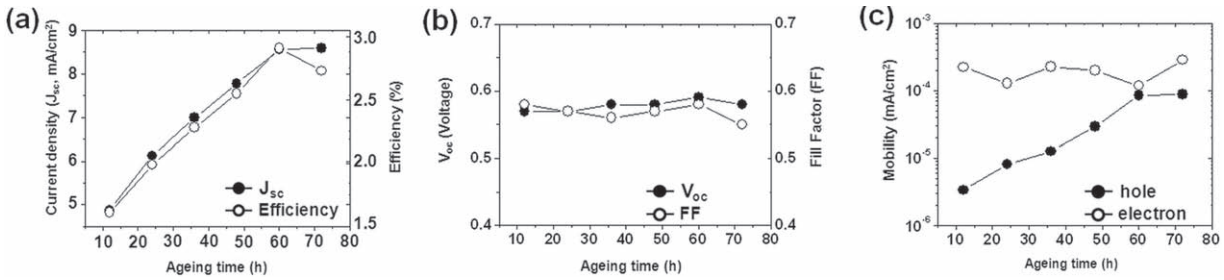

Figure 6. Dependence of (a) on the power conversion efficiency and J_{sc}, (b)V_{oc} and FF, and (c) hole-electron mobilities of P3HT nanowires/PCBM blend solar cells with various ageing times.

active layer. Finally, enhanced photovoltaic properties have been achieved. An optimum ageing time was found (60 h) for the P3HT nanowires. Very large P3HT aggregates form at ageing times longer than the 60 h limit, which may deteriorate the active layer and degrade the device properties.

Using the optimized P3HT nanowire ageing time, the effect of inserting a P3HT buffer layer between the ITO/PEDOT:PSS substrate and the P3HT nanowires/PCBM blended film was investigated (Figure 1c). With the P3HT buffer layer under the P3HT nanowires/PCBM blend active layer, the fabrication of a compositional-gradient cell (ITO/PEDOT:PSS/P3HT/P3HT nanowires:PCBM) was intended. The presence of a P3HT-only region will reduce the recombination loss at the active layer and the electrode. The device with the vertically-graded active layer including P3HT-only region between PEDOT:PSS and P3HT nanowire/PCBM blend layer minimizes the interfacial charge accumulation through energy-level matching, and also reduces energy losses for the transportation of holes to the anode. Additionally, wrong-way charge injection (such as electron injection to the ITO/PEDOT:PSS electrode) would be blocked by P3HT layer.[30]

Before spin-coating the P3HT nanowire/PCBM solution, a 15 nm P3HT layer was spin-coated onto the ITO/PEDOT:PSS electrode. Subsequently, the device was annealed at various temperatures (100 °C–250 °C) to enhance P3HT crystallization. The 60 h aged P3HT nanowire/PCBM blend solution was then introduced. Because the DCM used to suspend the P3HT nanowire/PCBM blend is a marginal solvent for pure P3HT, the pre-spin-coated P3HT layer was not fully dissolved. The increase in film thickness implies that the bottom layer thickness was unaffected and maintained its pre-spin-coated state. Although the P3HT layer was hydrophobic, the total thickness increased as observed for the coating of a single P3HT layer (15 nm). (In general, as the hydrophobicity of the bottom layer increased, the thickness of the over-coated layer decreased, **Table 2**). We attempted to insert a PCBM-only region at top the active layer to produce a compositional gradient cell (P3HT/PCBM). However, when DCM was used, the additional PCBM coating solution dissolved in the DCM and appeared to damage the PCBM portion of the P3HT nanowires:PCBM blend active layer. Therefore, poor device properties were obtained (data not shown).

Using this device, we investigated the (*J*–*V*) curves for the layered devices containing a P3HT/60 h aged P3HT nanowires:PCBM blend film as a function of the P3HT layer annealing temperature, shown in **Figure 8**. The P3HT layer annealed at 150 °C yielded the best performance with a J_{sc} = 10.27 mA·cm^{-2}, FF = 0.65, and a power conversion efficiency of 3.94%. SCLC measurements from the hole- and electron-only devices yielded the charge carrier mobilities of each device (Table 2). The device containing a P3HT layer annealed at 150 °C had very high hole and electron mobilities, (1.35×10^{-3} cm^2 V^{-1}s^{-1} and 3.45×10^{-3}cm^{2}V^{-1}s^{-1} respectively), and the mobility ratio between the hole and electron carriers was balanced by increases in the hole mobility. The balanced mobilities increased the FF for the optimized device structure (device containing a P3HT layer annealed at 150 °C, FF = 0.65). Because the accumulated SCLC charges were reduced by the increased hole mobility and enhanced charge collection efficiency, the fill factor is increased. We propose that the hole mobility difference between the P3HT nanowires in the upper layer and the

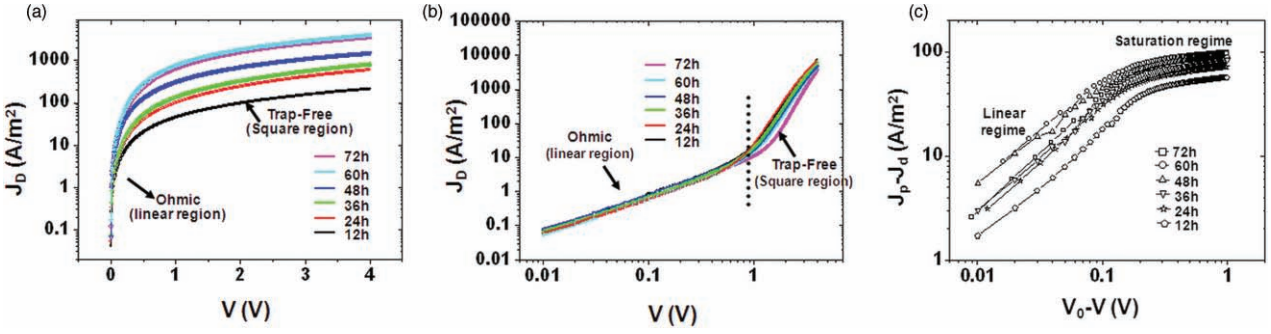

Figure 7. Experimental dark-current densities of P3HT nanowires/PCBM blend devices with various ageing times for (a) a hole-only device and (b) an electron-only device. c) Experimental photocurrent as a function of effective applied voltage (V_o–V) for various ageing times (12–72 h). V_o represents the compensation voltage for which the photocurrent J_{ph} = 0.

Table 2. Photovoltaic properties, charge carrier mobility of P3HT nanowires/PCBM blend films with various thermally-treated P3HT buffer layer.

Temperature [°C]	t [nm]	V_{oc} [V]	J_{sc} [mAcm^{-2}]	FF	η [%]	μ_h [cm^{2}V^{-1}s^{-1}]	μ_e [cm^{2}V^{-1}s^{-1}]	μ_e/μ_h
As prep.	93	0.57	9.78	0.58	3.22	1.30×10^{-4}	1.57×10^{-3}	12.1
100	94	0.57	9.98	0.61	3.44	5.28×10^{-4}	2.82×10^{-3}	5.3
150	92	0.59	10.27	0.65	3.94	1.35×10^{-3}	3.45×10^{-3}	2.6
200	95	0.57	9.91	0.63	3.59	8.48×10^{-4}	1.99×10^{-3}	2.3
250	91	0.52	2.57	0.57	0.76	4.60×10^{-5}	1.51×10^{-3}	32.8

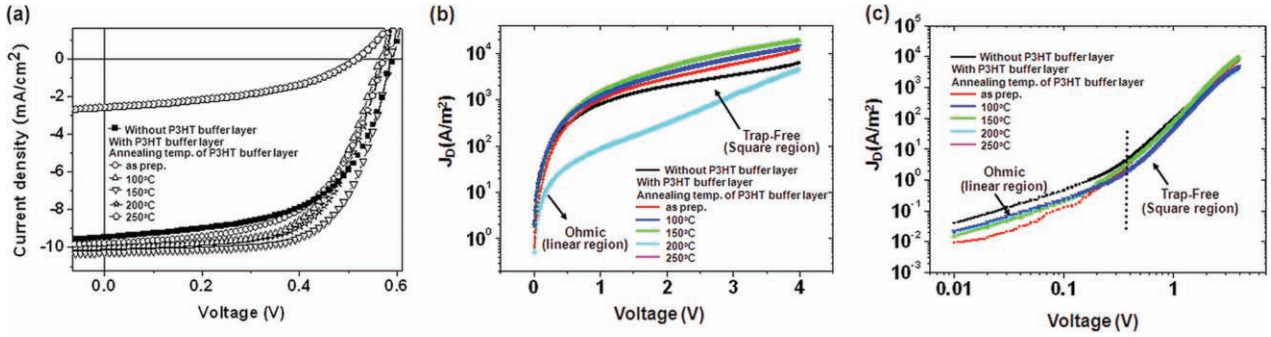

Figure 8. a) The current–voltage characteristics of P3HT nanowires/PCBM blend devices with various thermally-treated P3HT buffer layers, and the experimental dark-current densities for (b) a hole-only device and (c) an electron-only device.

annealed P3HT film layer at the bottom has decreased (the hole mobilities become comparable), which decreases the interfacial resistance of the layers between the P3HT buffer layer and the P3HT nanowires/PCBM blend active layer. As a result, the SCLC at the interfacial region of the film may have decreased. However, the device properties of films annealed at high temperatures, i.e., 200 °C and 250 °C, deteriorated. Because the surface roughness of the P3HT-only layer would be increased during the annealing process,[31] increased interfacial resistance between the pre-coated annealed layer and the additionally deposited layer limited charge transport, and the hole mobility of the device consequently decreased to a level on the order of 10^{-5} cm^2 V^{-1}s^{-1}. A pure donor phase (P3HT) layer at the hole collecting electrode (ITO) may minimize losses due to recombination of the wrong (opposite) charges at the electrode, as well as acting as a barrier to diffusion of the wrong charge carriers toward the respective electrodes. By insertion of the P3HT layer, electron back-transfer from the PCBM moieties to the ITO/PEDOT:PSS substrate is possibly blocked and, finally, enhanced electron mobilities relative to those of the P3HTnanowires/PCBM-only layer also could be achieved.

After further optimization including P3HT nanowires formation and blend morphology control, we expect to improve device performance and to approach more efficient bulk heterojunction architectures in the development of solar cell devices.

3. Conclusions

This work describes the optimization of a BHJ P3HT nanowires/PCBM photovoltaic cell created via solution crystallization in DCM. The photovoltaic properties of P3HT nanowires/PCBM blend as a function of solution ageing time were studied. The best device performance was achieved using a device coated with a 60 h aged P3HT nanowires/PCBM blend solution. TEM, AFM, and GI-XRD studies showed that the optimized photovoltaic properties (η = 3.23%) arose from the formation of an interconnected network of highly oriented P3HT nanowires self-assembled with PCBM. The photovoltaic properties, particularly the short circuit current density, depend strongly on the ageing time of the P3HT precursor solution. We found that the optimum conditions, in which light absorption was maximized and the carrier mobility was balanced, occurred at 60 h ageing time. We propose a new device architecture containing a pure donor phase layer inserted between the ITO/PEDOT:PSS and P3HT nanowires/PCBM layers. Using the optimized annealing conditions for the P3HT buffer layer (150 °C), a high hole mobility on the order of 1.35×10^{-3} cm^2 V^{-1}s^{-1} was observed by SCLC measurements, and a power conversion efficiency of 3.94% was achieved. A compositionally-graded cell that included a P3HT-only region showed reduced charge recombination by injection of the wrong charge to the electrodes, and this structure enhanced the device properties. Further optimizations of this device are necessary to increase the performance of devices composed of semiconducting polymer nanowires.

4. Experimental Section

Regioregular P3HT (Mn = 37k, PDI = 2.0, RR = 90%–93%) and PCBM (99.5%) used in this study were obtained from Rieke Metals and Nano-C Inc., respectively. All materials were used as received without further purification.

Devices were fabricated on indium tin oxide (ITO)-coated substrates. After cleaning the ITO substrates with detergent (Mucasol), acetone, and isopropyl alcohol, a layer of poly(3,4-ethylenedioxythiophene)-poly(styrene sulfonate) (PEDOT-PSS, Baytron P TP AI 4083, Bayer

AG) was spin-coated to a thickness of 30 nm and baked at 120 °C in a convection oven for 30 min. A P3HT/PCBM solution (1:1 by weight) was blended in dichloromethane (DCM, CH_2Cl_2) to a concentration of 4 mg·mL^{-1} at 42 °C, and the solution was cooled down to room temperature. Subsequently, the solution was stirred for ageing times of 12 h-72 h. After ageing, the solutions were spin-coated onto the PEDOT:PSS-coated ITO substrate.

The pure P3HT layer was applied to the active layer/electrode interface by spin-coating the P3HT solution dissolved in chlorobenzene at a concentration of 0.5 wt% (15 nm) onto the PEDOT:PSS-coated ITO substrate before depositing the active layer. Subsequently, the devices were annealed at various temperatures (100 °C-240 °C) and the aged P3HT nanowire/PCBM blend DCM solutions were coated over this as an active layer. An ageing time of 60 h was experimentally determined to be optimal.

Efficiency measurements were conducted using a thermally-deposited Ca (20 nm)/Al (80 nm) cathode. Hole-only/electron-only devices were fabricated with PEDOT:PSS/Pd and Al/Al electrodes as the anodes/cathodes to measure the electron and hole mobilities. The electrical characteristics were measured using Keithley 4200 source/measure units in the dark and under AM1.5 solar illumination (Oriel 1 kW solar simulator) referenced using a Reference Cell PVM 132 calibrated at NREL at an intensity 100 mW·cm^{-2}. The incident photon-to-current conversion efficiency (IPCE) was measured as a function of the wavelength using a photomodulation spectroscopic setup (model Merlin, Oriel). All electrical measurements were performed in an O_2-purged glove box under inert N_2. The film morphologies were characterized using the phase mode of an atomic force microscope (AFM, DI, Nanoscope III), field-emission scanning electron microscope (FESEM, Hitachi S-4800), and transmission electron microscope (TEM, Hitachi H-7600). Grazing-incidence X-ray diffraction (GI-XRD) measurements were performed at the 3C2 beam line (wavelength 1.107 Å) of the Pohang Accelerator Laboratory (PAL). The angle between the film surface and the incident beam was fixed at 0.18°. The measurements were obtained at scanning intervals of 2θ between 3° and 25°. Solution UV-vis absorption spectra were recorded at various temperatures with a cooling rate of 0.1 °C·min^{-1} from 42 °C using an Agilent 8453 (HP) UV-vis spectrophotometer with an equilibrium time of 30 min. Solid UV data were obtained using the same apparatus.

Supporting Information

Supporting Information is available from the Wiley Online Library or from the author.

Acknowledgements

This work was supported by the National Research Foundation of Korea grant (No. 2009–0093485) and Energy R&D program (20093020010040) under the Korea Ministry of Knowledge Economy. The authors thank the Pohang Accelerator Laboratory for providing the synchrotron radiation sources at 4C2, 8C1 and 10C1 beam lines used in this study.

Received: May 15, 2010
Revised: August 25, 2010
Published online: November 23, 2010

[1] Y. Kim, S. Cook, S. M. Tuladhar, S. A. Choulis, J. Nelson, J. R. Durrant, D. D. C. Bradley, M. Giles, I. McCulloch, C.–S. Ha, M. Ree, *Nat. Mater.* **2006**, *5*, 197.
[2] A. J. Mozer, N. S. Sariciftci, *Chem. Phys. Lett.* **2004**, *389*, 438.
[3] G. Yu, J. Gao, J. C. Hummelen, F. Wudl. A. J. Heeger, *Science* **1995**, *270*, 1789.
[4] N. S. Sariftci, L. Smilowitz, A. J. Heeger, *Science* **1992**, *258*, 1474.
[5] W. Ma, C. Yang, X. Gong, K. Lee, A. J. Heeger, *Adv. Funct. Mater.* **2005**, *15*, 1617.
[6] K. M. Coakley, M. D. McGehee, *Adv. Funct. Mater.* **2001**, *11*, 15.
[7] J. Peet, J. Y. Kim, N. E. Coates, W. L. Ma, D. Moses, A. J. Heeger, G. C. Bazan, *Nater. Mater.* **2007**, *6*, 497.
[8] G. Li, V. Shrotriya, J. S. Huang, Y. Yao, T. Moriarty, K. Emery, Y. Yang, *Nat. Mater.* **2005**, *4*, 864.
[9] A. J. Moule, K. Meerholz, *Adv. Mater.* **2008**, *20*, 240.
[10] M. C-. Quiles, T. Ferenczi, T. Agostinelli, P. G. Etchegoin, Y. Kim, T. D. Anthopoulos, P. N. Stavrinou, D. D. C. Bradley, J. Nelson, *Nat. Mater.* **2008**, *7*, 158.
[11] B. C. Thompson, B. J. Kim, D. F. Kavulak, K. Sivula, C. Mauldin, J. M. J. Frechet, *Macromolecules* **2007**, *40*, 7425.
[12] F. Padinger, R. S. Rittberger, N. S. Sariciftci, *Adv. Funct. Mater.* **2003**, *13*, 85.
[13] Y. Kim, S. Cook, J. Kirkpatrick, J. Nelson, J. R. Durrant, D. D. C. Bradley, M. Giles, M. Heeny, R. Hamilton, I. McCulloch, *J. Phys. Chem. C* **2007**, *111*, 8137.
[14] H.-L. Yip, S. K. Hau, N. S. Baek, H. Ma, A. K.-Y. Jen, *Adv. Mater.* **2008**, *20*, 2376.
[15] J. S. Kim, J. H. Park, J. H. Lee, J. Jo, D.Y. Kim, K Cho, *Appl. Phys. Lett.* **2007**, *91*, 112111.
[16] X. Yang, J. Loos, S. C. Veenstra, W. J. H. Verhees, M. M. Wienk, J. M. Kroon, M. A. J. Michels, R. A. J. Janssen, *Nano Lett.* **2005**, *5*, 579.
[17] A. M. Ballantyne, L. Chen, J. Dane, T. Hammant, F. M. Braun, M. Heeney, W. Duffy, I. Mulloch, D. D. C. Bradley, J. Nelson, *Adv. Funct. Mater.* **2008**, *18*, 2373.
[18] S. Berson, R. Bettignies, B. Severine, G. Stephane, *Adv. Funct. Mater.* **2007**, *17*, 1377.
[19] L. Li, G. Lu, X. Yang, *J. Mater. Chem.* **2008**, *18*, 1984.
[20] H. Xin, F. S. Kim, S. A. Jenekhe, *J. Am. Chem. Soc.* **2008**, *130*, 5424.
[21] H. Xin, G. Ren, F. S. Kim, S. A. Jenekhe, *Chem. Mater.* **2008**, *20*, 6199.
[22] L. Qiu. W. H. Lee, X. Wang, J. S. Kim, J. A. Lim, D. Kwak, S. Lee, K. Cho, *Adv. Mater.* **2008**, *21*, 1349.
[23] L. Qiu, X. Wang, W. H. Lee, J. A. Lim, J. S. Kim, D. Kwak, K. Cho, *Chem. Mater.* **2009**, *21*, 4380.
[24] V. D. Mihailetchi, H. Xie, B. de Boer, L. J. A. Koster, P. W. M. Blom, *Adv. Funct. Mater.* **2006**, *16*, 699.
[25] Y. Zhao, Z. Xie, Y. Qu, Y. Geng, L. Wang, *Appl. Phys. Lett.* **2007**, *90*, 043504.
[26] M. A. Lampert, P. Mark, *Current injection in Solids*; Academic Press: New York **1970**.
[27] L. J. A. Koster, E. C. P. Smits, V. D. Mihailetchi, P. W. M. Blom, *Phys. Rev. B* **2005**, *72*, 085205.
[28] J. H. Park, J. S. Kim, J. H. Lee, W. H. Lee, K. Cho, *J. Phys. Chem. C* **2009**, *40*, 17579.
[29] V. D. Mihailetchi, J. Wildeman, P. W. M. Blom, *Phy. Rev. Lett.* **2005**, *94*, 126602.
[30] A. Kumar, G. Li, Z. Hong, Y. Yang, *Nanotechnology* **2009**, *20*, 165202.
[31] G. Li, V. Shrotriya, Y. Yao, Y. Yang, *J. Appl. Phys.* **2005**, *98*, 043704.